SUPPORTING INFORMATION:

LARGE-SCALE METASURFACES MADE BY AN EXPOSED RESIST

Daniel Andrén[†,*], Jade Martínez-Llinàs[†], Philippe Tassin[†], Mikael Käll[†], Ruggero Verre[†,*]

[†]*Department of Physics, Chalmers University of Technology, S-412 96 Gothenburg, Sweden*

**Corresponding authors: daniel.andren@chalmers.se, mikael.kall@chalmers.se, ruggero.verre@chalmers.se*

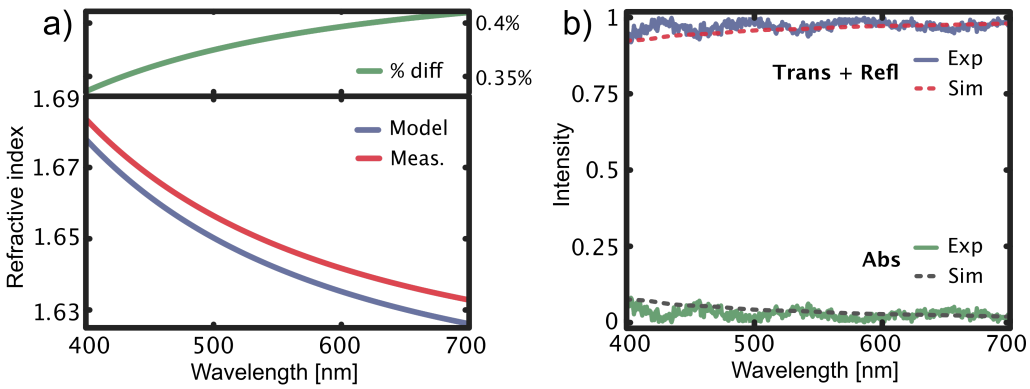

Figure S1: Optical parameters of the ma-N 2410 resist. a) Refractive index of the resist as described by the Cauchy parameters (A = 1.601, B = 0.123) and experimentally measured using ellipsometry. The top inset shows the percent error between the model and measured refractive index. b) Experimentally measured transmission, reflection, and absorption of a 1 µm thick ma-N continuous film (solid lines), showing <5% absorption in the visible wavelength regime. From this the imaginary part of the refractive index of the material, responsible for wave attenuation, is estimated to be decaying from 0.0025 to 0.001 in the visible wavelength range. Using this imaginary part of the RI in an FDTD simulation of the optical interaction in a 1 µm thick film of ma-N qualitatively reproduces the experimentally measured interaction. Hence, this complex refractive index is used in subsequent FDTD simulations of the meta-atoms.

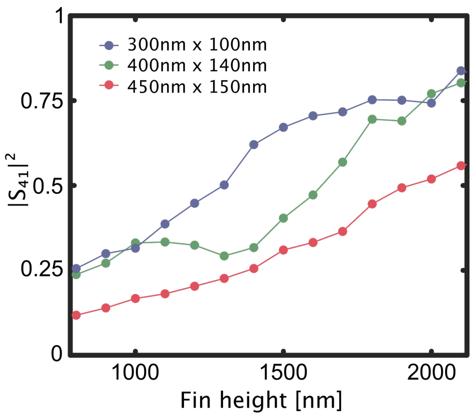

Figure S2: Simulated cross-polarized transmission efficiency versus fin height. The taller the nanofin, the higher the efficiency of the phase gradient metasurface.

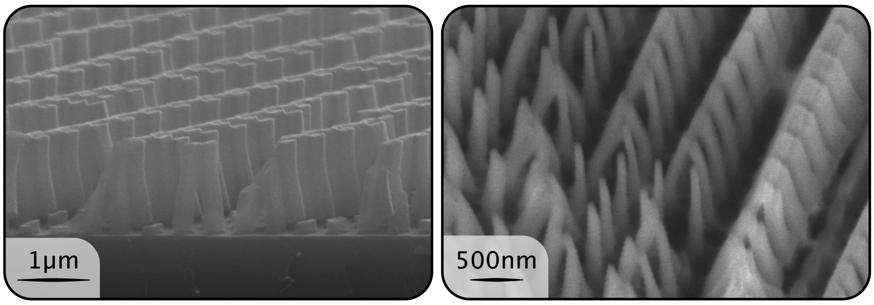

Figure S3: High aspect ratio nanofins dried from water with nitrogen gun. Interfacial forces at the water-air interface create stresses sufficient to collapse tightly packed, high aspect ratio nanofins. The SEM images above display two examples of samples where fins have collapsed during drying of rinse water. To obtain tightly packed larger aspect ratio nanofins, providing metasurfaces with high efficiencies, critical point drying is used. This successfully prevents pattern collapse (see **Figure 2a** in main text).

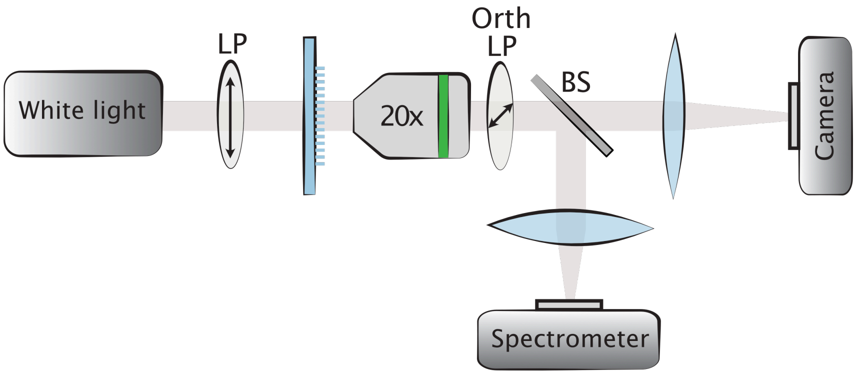

Figure S4: Experimental setup for polarization conversion efficiency. The metasurface sample is placed between crossed linear polarizers. The metasurface sample is mounted on a rotation stage that allows the metasurface to be arbitrarily rotated with respect to the linear polarizers. The transmitted light is passed through a beamsplitter and guided to a spectrometer and a camera, respectively. During an experiment, the samples are oriented with the nanofins aligned at 45° from the Cartesian axis of a periodic array. Since these metasurfaces function as a half-wave plates, they will, when oriented with their fast axis at 45° from the incoming linear polarization, rotate the direction of polarization by 90°, and allow light to pass through the second orthogonal linear polarizer.

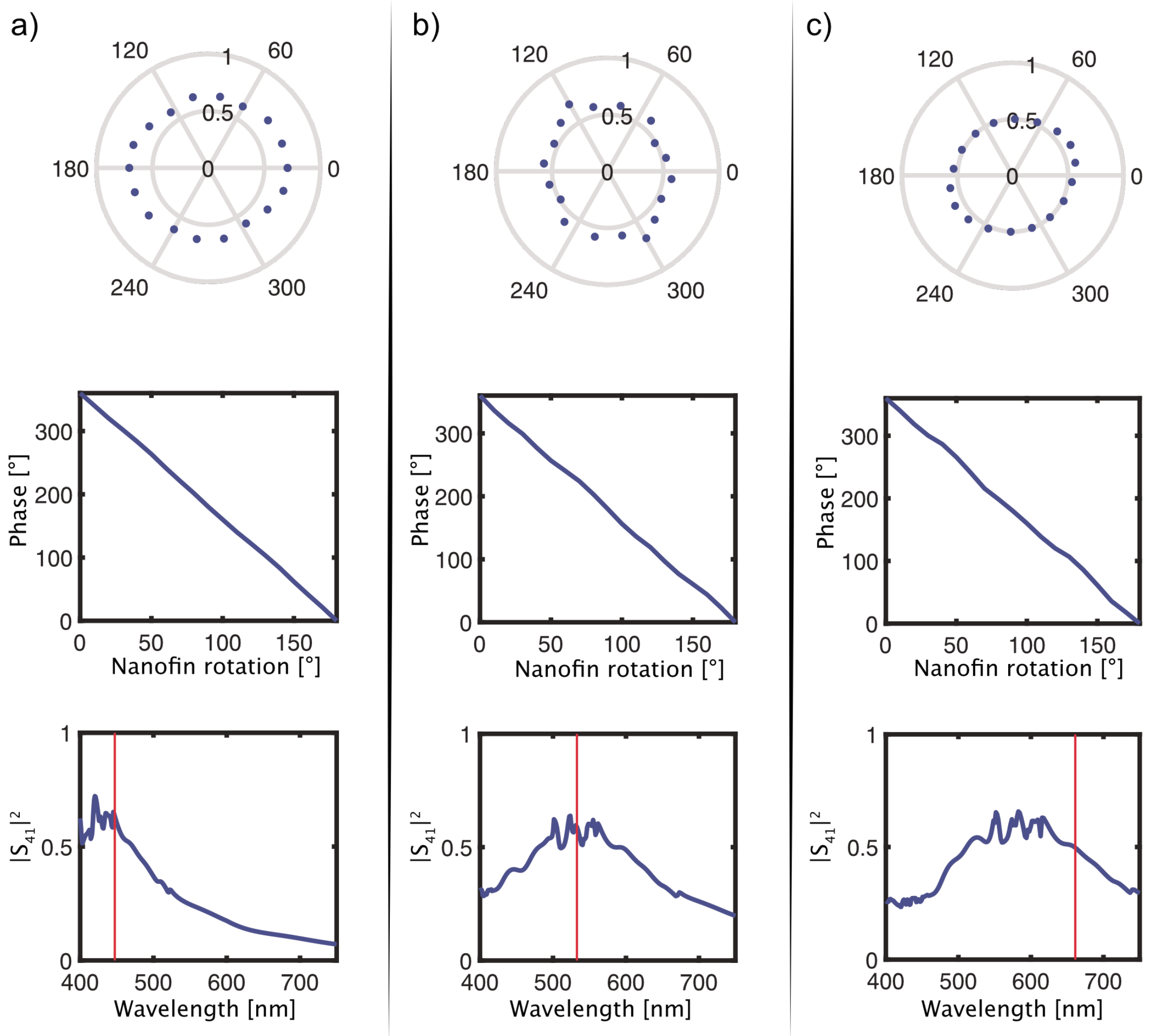

Figure S5: Simulation details for the resist metasurfaces. FDTD simulations of meta-atoms in periodic boundary conditions and with different rotation angles. Three different sizes of meta-atoms are optimized for different wavelength regions: 100nm x 300nm x 1400 nm for 447 nm (a), 140nm x 400nm x 1700 nm for 532 nm (b), and 150nm x 450nm x 1900 nm for 660 nm (c). The radial plot (top panels) displays induced phase for different orientations of meta-atoms versus the magnitude of the $|S_{41}|^2$ parameter (i.e. transmission efficiency for light of opposite handedness from the incoming light). It is here observed that within a π rotation of the meta-atom, full 2π phase manipulation is possible with approximately constant intensity. Moreover, the relation between nanofin rotation angle and induced phase difference is close to linear (middle panels), allowing the use of the $\varphi = 2\theta$ relation to build up any desired phase profile. Lastly, the $|S_{41}|^2$ spectra (bottom panels) are displayed for reference, illustrating the wavelength-tunability of potential resist metasurfaces, depending on the design parameters.

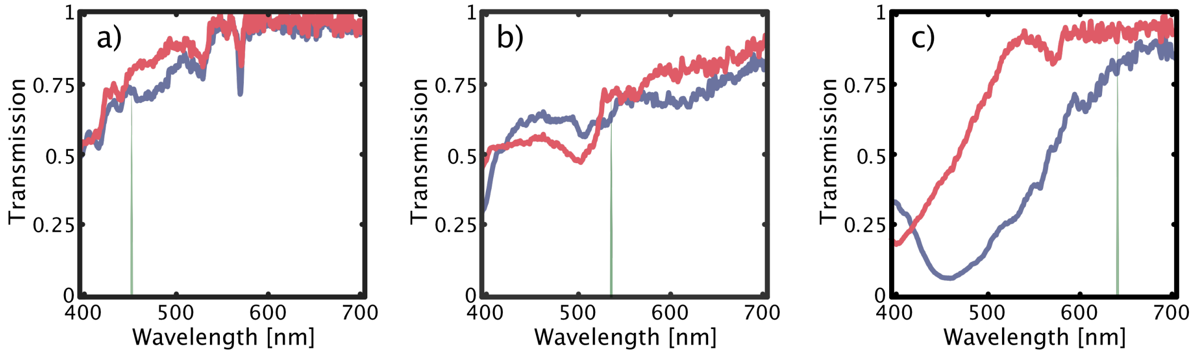

Figure S6: Measured linearly polarized transmission through nanofin arrays. Experimental transmission values measured for light linearly polarized along the long and short axis of the nanofins. The fact that the transmission for polarization along the short and long axis of the elongated nanofins are similar in the optimized wavelength range (blue, green, or red) indicates that it is shape birefringence rather than anisotropic absorption that induces the polarization conversion observed experimentally. The different graphs show transmission spectra for unit-cell dimensions: a) 300nm x 100 nm, b) 400nm x 140nm, and c) 450nm x 150nm. The laser wavelengths (447, 532, and 660 nm) used to subsequently study the different metasurfaces are indicated by vertical lines in the respective figure.

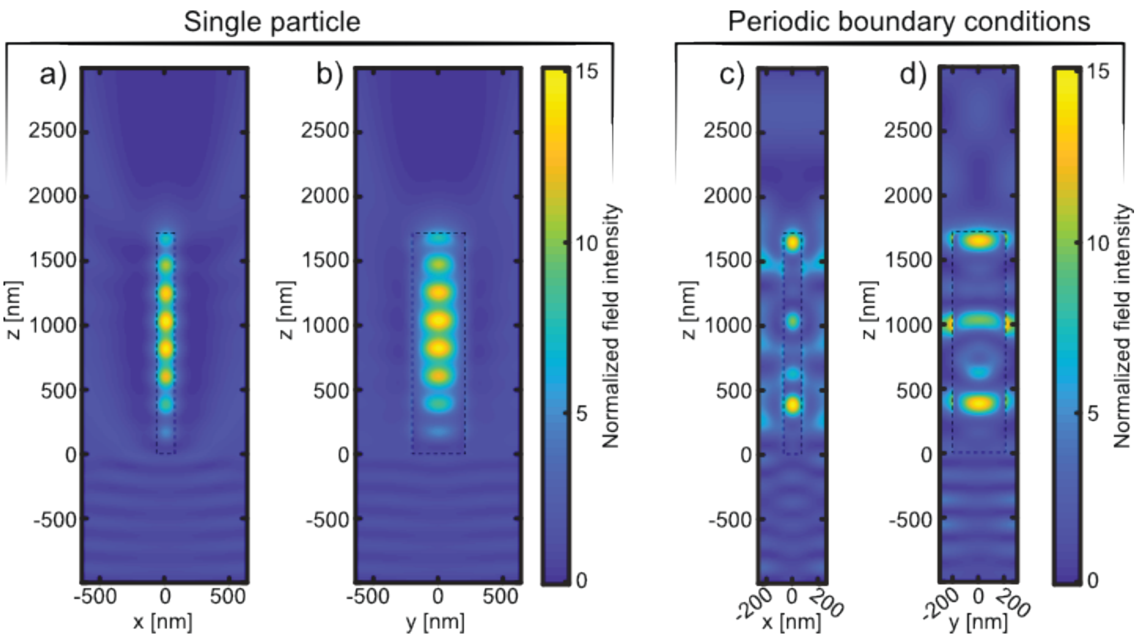

Figure S7: Meta-atoms and surfaces exhibiting multimodal waveguiding properties, in line with "propagation delay"-metasurfaces. a) and b) show calculated electric field intensity plane cuts at the wavelength 532 nm along the short and long principal axes, respectively. For these, a single meta-atom is excited by a plane wave incident from below, and the unperturbed pure waveguide mode supported by the nanoparticle is visible. c) and d) display the same physical quantity, but the boundary conditions in the x and y directions are periodic, simulating the behavior of a metasurface. Due to near-field coupling, part of the mode is guided in the air gap between adjacent particles, but nevertheless the waveguiding property remains. In all figures, a dashed box is drawn to indicate the physical extent of the nanofin.

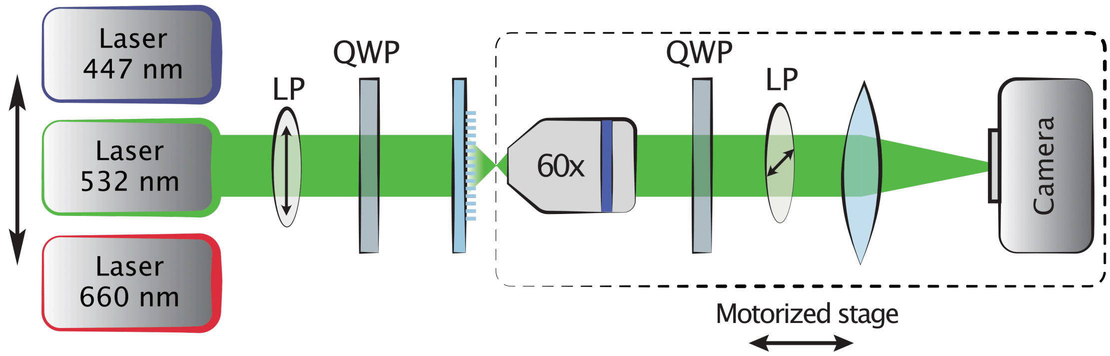

Figure S8: Experimental setup for characterizing the focus profile of the transmissive metalenses. Three different lasers (blue, green and red) can via fiber-coupling be made to enter the beam path. After circularly polarizing the laser light with a quarter wave-plate, the light is passed through a metalens to form a focus. On the opposite end of the setup an imaging system is constructed on a motorized stage. The polarization optics on this stage is aligned to select for the opposite handedness to the incoming light. By scanning the motorized stage, one can map the intensity profile of the focused beam along the optical axis.

In order to characterize this metalens efficiency with spectral resolution, the laser light source is replaced by a white-light source. A liquid crystal tuneable filter is used to perform hyperspectral imaging, and the copolarized light impinging on the same area as the metalens is used to normalize the efficiency measurement. By using polarization optics to select for each handedness of circular polarization it is possible to measure the efficiency spectra of the metalenses.

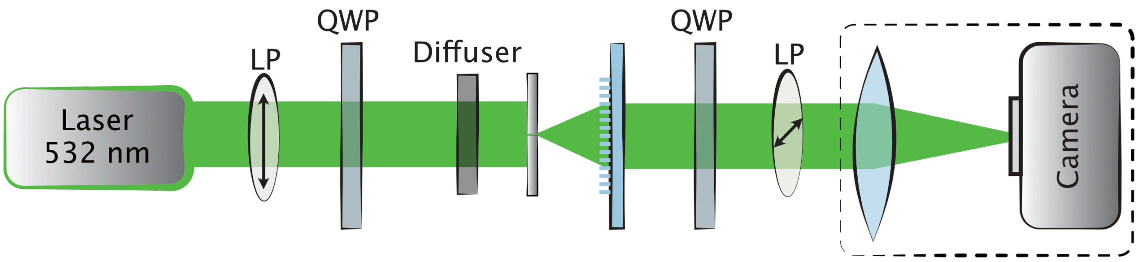

Figure S9: Experimental setup for imaging with the transmissive metalens. Polarization optics is aligned to select one handedness of the incident light and the opposite handedness of the transmitted light, as in Fig. S7, but the imaging lens/objective is now replaced by the metasurface. Furthermore, a diffuser is inserted into the beam path to remove any speckles induced by the laser illumination. The components within the dashed box can be removed in order to instead project the image onto a screen for increasing the field of view.

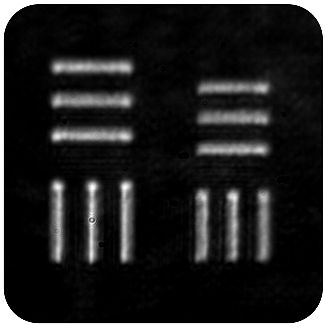

Figure S10: Imaging of a standardized resolution test chart (1951 USAF). Representative image formed using the metalens to study the most detailed pattern on the resolution test chart. The smallest features of this chart are the rightmost lines (2.2 µm wide and spaced by 4.4 µm)

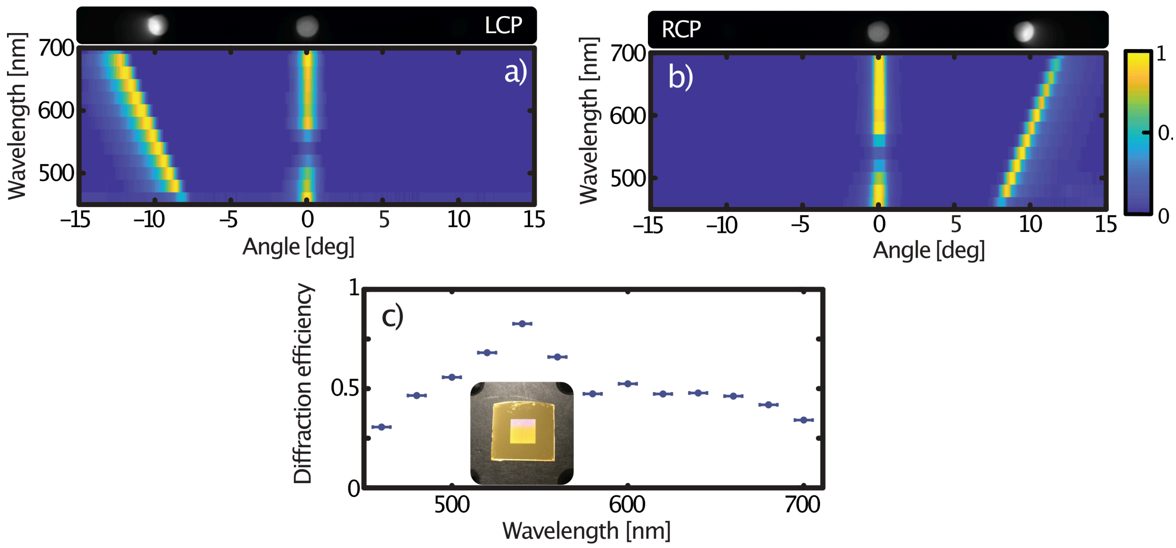

Figure S11: A linear phase gradient metasurface fabricated on a gold mirror. Experiments similar to those performed in Figure 4c-e) in the main text, but for a metasurface built on a sputtered 100 nm gold film. The sample is characterized using the hyperspectral Fourier imaging set-up illustrated in Fig. S11. The wavelength dependent reflection angles for left- and right-handed circularly polarized light are presented in a) and b), respectively. The top insets show Fourier images for the wavelength with highest diffraction efficiency, at around 550 nm. c) Diffraction efficiency, defined as the intensity ratio between the preferred 1st order and the 0th order (specular reflection). The inset shows the 8mm x 8mm metasurf ace on a gold mirror sample used in the experiment.

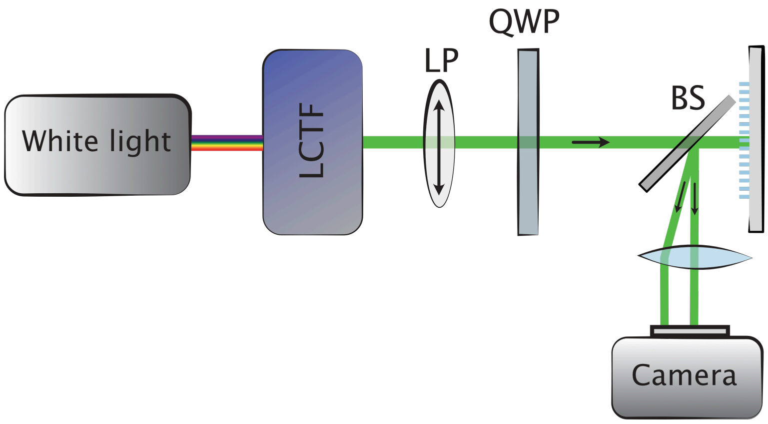

Figure S12: Experimental setup for characterizing the reflective phase gradient metasurface. A hyperspectral imaging system based on white light filtered through a liquid crystal tunable filter (LCTF, Varispec 420-730 nm) is used. The incident color selected light is circularly polarized and reflected from a linear phase gradient metasurface fabricated on a mirror, which thus acts as a blazed reflection grating. The different diffraction orders are characterized by angle resolved Fourier imaging after being selected by a beamsplitter.

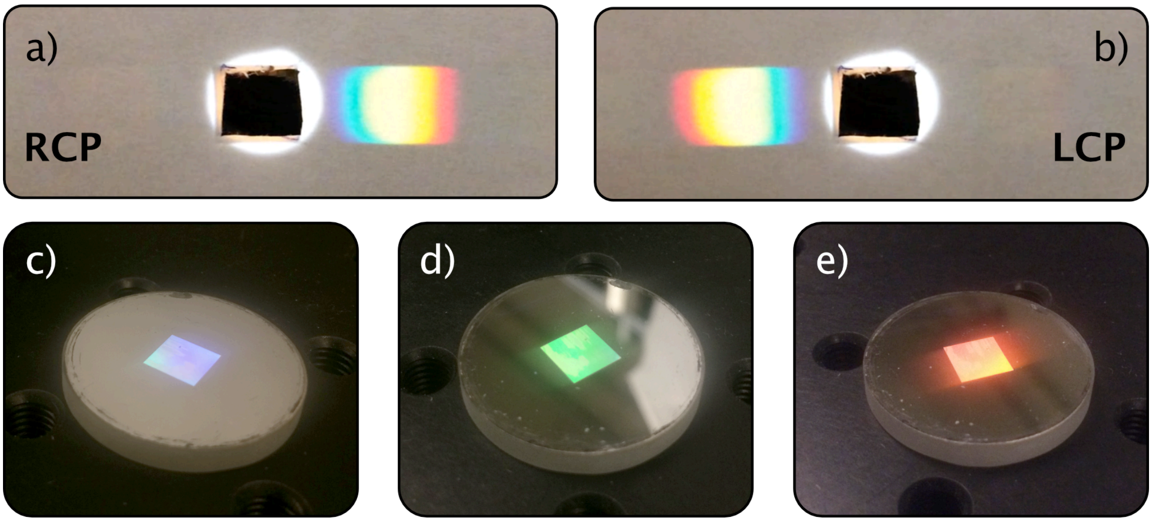

Figure S13: Macroscopically observable chromatically resolved angular dispersion of light from the reflective metasurface. Panels a) and b) demonstrate photographs taken by the authors of the spectrum formed by collecting the reflection of incoming white light on a screen for either right- or left-handed circular polarization. Panels c)-e) illustrate the different colors observed for different viewing angles using ambient light conditions in the lab.